Composite Structures 192 (2018) 368–378

Contents lists available at ScienceDirect

Composite Structures

journal homepage: www.elsevier.com/locate/compstruct

Development of full carbon wheels for sport cars with high-volume technology

Francesco Rondina[a], Sara Taddia[a], Laura Mazzocchetti[a], Lorenzo Donati[a], Giangiacomo Minak[a,*], Philipp Rosenberg[b], Andrea Bedeschi[c], Enrico Dolcini[c]

[a] CIRI MAM, Alma Mater Studiorum - Università di Bologna, Italy
[b] Fraunhofer Institute for Chemical Technology, ICT Pfinztal, Germany
[c] Riba Composites S.r.l., Faenza, Italy

ABSTRACT

Aim of the paper is to present the methodology used to develop a new process, based on high-pressure resin transfer molding (HP-RTM), to produce full carbon reinforced plastic rims for sports car. These components are nowadays made by pre-preg autoclave processing, which is expensive and time-consuming, so that they are basically sold as aftermarket option. The proposed technology allows a manufacturing volume high enough to be suitable for series production. In this paper, the resin and fiber selection criteria and tests are shown, as regards the mechanical properties, durability and injection strategies.

1. Introduction

Weight of cars increased continuously through the years up to 2010, in relation to improvements in comfort, driving aid systems and the more challenging homologation passive safety requirements. Since 2000 an increasing attention towards weight reduction in all car segments was adopted by all OEM (Original Equipment Manufacturer) as consequence of increasing requirements on pollution emissions reduction. Indeed, despite the development of more efficient engines, the higher fuel consumption, and consequently higher CO_2 emissions, due to weight have required the intervention from the governments (in particular US and EU) to set a path for emission reduction through the years [1].

Research into lightweight components, materials and the related processes, has therefore become one of the main challenges in the automotive industry and has led to the substitution of standard steel with alternative materials in many components and systems. Typically, steel was first substituted by aluminium, but OEM are now looking at carbon fibre-reinforced plastics (CFRP) technologies for their premium models, since they offer further weight reduction together with higher specific stiffness. This trend will also be particularly important for next-generation hybrid or electric vehicles. Indeed, CFRP are not only lightweight and high-strength but they can also be tailored in order to improve structural, functional or cosmetic properties. The market size for CFRP composites accounted for $20.3 billion in 2014, and is projected to register a compound annual growth rate (CAGR) of 9.9% between 2015 and 2020, to reach $35.8 billion [2]. CFRPs were traditionally used in the aerospace, defence industry or in racing applications but today they are finding new uses in automotive, marine, energy (e.g. for wind blades), industrial components and other sectors [3]. Automotive is the most promising application field for composites, and offers the highest growth potential. Many leading automotive manufacturers, such as BMW and Mercedes, are planning or have already started to scale-up their production of fuel-efficient cars through weight reduction by using carbon fibres. These efforts are projected to drive the CFRP market in the automotive industry, making it the leading industry by 2020 [2].

Several factors are driving the automotive market but the costs are, still today, a major barrier. If the cost of raw carbon fibre is following a decreasing trend, the manufacturing costs are instead almost constant if conventional high-performance technologies are used (i.e. autoclave processing). Moreover several composite technologies cannot provide a component cost reduction by increasing the production volume (series production). To achieve a reliable component-cost reduction, new out-of-autoclave technologies (like infusion technologies, prepreg compression technologies or short fibre compound processing) have been recently optimized and they are now ready for industrial use. Among the others High-Pressure Resin Transfer Moulding technology (HP-RTM) seems to be the most promising technologies to produce complex components with high performance at high volume rates.

The “classic” Resin Transfer Moulding process (RTM) can be successfully applied for the manufacturing of high-performance structural

* Corresponding author.
E-mail address: giangiacomo.minak@unibo.it (G. Minak).

https://doi.org/10.1016/j.compstruct.2018.02.083
Received 13 January 2018; Accepted 27 February 2018
Available online 06 March 2018
0263-8223/ © 2018 The Authors. Published by Elsevier Ltd. This is an open access article under the CC BY license (http://creativecommons.org/licenses/BY/4.0/).

automotive components based on continuous fibre reinforced composites. The dry three-dimensional preform is placed into the mould cavity and resin-hardener mixture is injected at low pressure of 1 to 20 bar into the closed mould. The pressure, together with fibre permeability, is able to produce components with 50% and higher fibre volume fraction, thus providing excellent mechanical properties [4–7]. Nevertheless, in the classical RTM process, the low flow rate of resin and low injection pressure results in long resin injection time thus hampering the use of fast cure resins and consequently the overall productivity. As consequence, the "classic" RTM process is mainly limited to low-volume manufacturing capacity and, only to a minor extent, to slightly lower mechanical proprieties related to lower fibre volume fraction. High volume manufacturing with RTM is possible only if the process cycle time is reduced significantly. With High Pressure RTM equipment, the resin system can be injected in the mould cavity with high flow rates. The combination of high-pressure pumps for dosing resin and hardener, and self-cleaning mixing head of such equipment guarantee precise resin and hardener mixing along with materials injection into the mould at constant defined flow rate (20–200 g/s) though high flow resistance is created in the mould cavity [8]. In order to further reduce the process cycle duration, an automated or semi-automated preforming phase is usually added: dry reinforcements are automatically cut and stacked in the desired stacking sequence, which is then draped to generate a 3-d preform for further resin injection in the HP-RTM mould. A scheme of the HP-RTM process chain is shown in Fig. 1.

Stating this scenario, the Italian company Riba Composites, Fraunhofer ICT and LBF research centres (Germany), Alpex Technologies GmbH (Austria), University of Bologna (Italy) and TUV-Sud (Germany) set up a research project within the European Horizon 2020 programme with the acronym CARIM [9]. The consortium was funded in the call Fast Track to Innovation (FTI) to design, develop and validate a high-volume process chain for the production of automotive wheel made in carbon fibre reinforced plastic. An automated preforming and HP-RTM process will ensure short cycle times and lower costs compared to conventional composite technologies. This ensures the scale-up to series production to make the CARIM wheels competitive and lighter than current casted and forged Al-wheels and other emerging plastic wheel concepts. Short term goals of the project are the validation of an industrial process chain able to produce 30% lighter than state-of-the-art forged Al-wheels, and 50% lighter than conventional cast Al-wheels, a short cycle times (i.e. 30 min/wheel component – with goal to reduce to 15 min in 2020) thus allowing a competitive cost respect to forged and casted Al-wheels, with an annual production target of 10,000–20,000 pieces per year (Fig 2).

This paper introduces the concept of the methodology underlying the first steps of the CARIM project and presents the preliminary results. The starting point of the project was the selection of resin systems and fibres for the set-up of an HP-RTM process chain. The selection was made based on the process requirements and the desired mechanical properties. The reference product was a pre-preg based wheel produced in hand-layup/autoclave technology by Ri.Ba. that had already passed several homologation tests. The selection of the injection strategy with a process simulation FEM approach [7,10] (ESI PAM-Composites) concludes this initial project phase.

2. Materials and methods

2.1. Process parameters

The selection of the fibre and resin systems has to match several and often conflicting requirements in relation to the selected manufacturing process chain, of the required production rates, of the expected performance of the final component and to the environmental aging of everyday use of the component.

In particular the resin system is required to have: low viscosity, short curing time, compatibility with HP-RTM equipment, good durability, a glass transition temperature (T_g) above a critical level, good static and fatigue properties also after exposure to harsh environmental conditions. Analogously, the fibre and fibre layup were required to keep a good permeability also for HP-RTM application, a good drapability, to exhibit good mechanical properties for typical operative loads.

Following the selection phase of materials suitable for the wheel application, two different RTM resin systems were preliminary evaluated: system H2.2 (anhydride-based hardener) and system H4 (amine-based hardener). For comparison, the ER450 system used for the prepreg/autoclave cured prototype already produced, was also included in the evaluation. Plates were produced with all the resin candidates using the same fibre type 12K T700 2 × 2 twill with 630 g/m^2 areal weight; a plate layup $[(0/90)]_8$ was chosen based on the basis of subsequent material testing specification to reach a final thickness around 5 mm. Details are shown in Table 1.

The prepreg plate was hand layup and cured in autoclave for 2 h at 135 °C under 6 bar pressure; post-curing of the whole plate at 200 °C for 2 additional hours was done in oven under recirculating air. The RTM

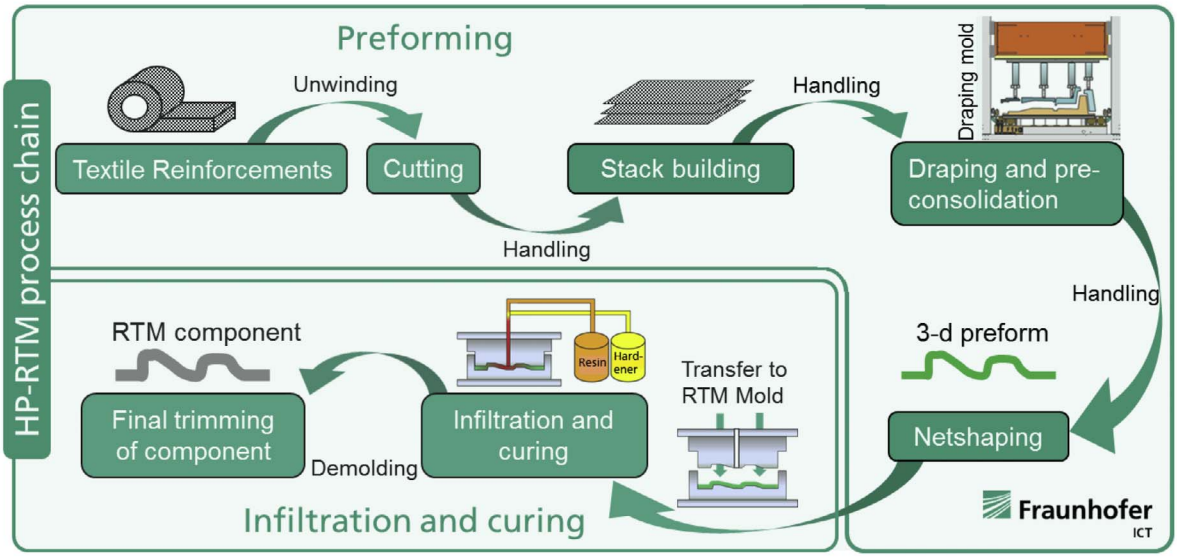

Fig. 1. HP-RTM process chain for manufacturing of high-performance composites.

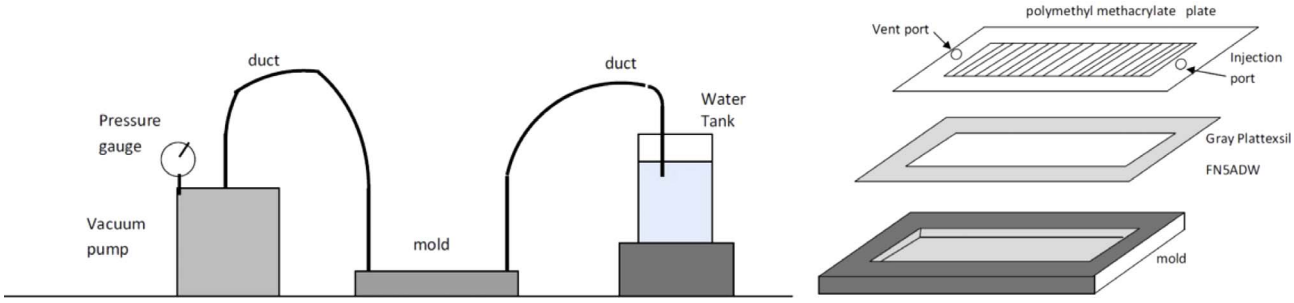

Fig. 2. Permeability characterization testing set-up.

Table 1
Plate production, selection of materials.

Materials	Process	Cure cycle	Post-cure cycle	Final thickness
ER450	Vacuum + 6 bar autoclave cure	2 h @ 135 °C	2 h @ 200 °C	5.02 mm
H2.2	5 bar closed mould RTM	30 min @ 120 °C	24 h @ 180 °C	4.84 mm
H4	5 bar closed mould RTM	90 min @ 80 °C	1 h @ 150 °C, 3 h @ 180 °C, 1 h @ 200 °C	4.83 mm

plates were produced as follows: the injection layout consists in a resin track all around the plate and central vent. An injection pressure of 5 bar was applied together with vacuum at the vent. Different cure cycles were realized for systems H2.2 and H4 as reported in Table 1. The plates were finally waterjet cut for the extraction of the specimens of the required dimensions for testing.

The plates were characterized by Differential Scanning Calorimetry (DSC), Thermogravimetric analyses (TGA) and Dynamic-Mechanical Analysis (DMA). Differential Scanning Calorimetry measurements were carried out on a TA Instruments DSC Q2000 apparatus equipped with RCS cooling system, heating twice 3–5 mg samples in aluminium pans from 0 °C to 350 °C at 10 °C/min, with intermediate cooling run carried out at −10 °C/min. Thermogravimetric analyses were carried out on a TA Instruments SDT Q600, in air atmosphere (flow rate: 100 ml/min) heating from 25 °C to 600 °C at 10 °C/min, followed by 30 min isotherm. DMA was performed with a NETZSCH 242 E Artemis analyser in three-point bending configuration with a 40 mm span, with 1 Hz oscillation frequency and 20 µm oscillation amplitude, heating from RT up to 250 °C at 3 °C/min heating rate; samples for DMA are about 50x5x5mm (the exact dimensions were measured for each coupon).

2.2. Mechanical and durability testing

Concerning the mechanical characterization, the most critical failure mechanisms for composite materials subjected to a complex loading history are the ones dominated by the matrix, both in-plane and out of plane (intra-ply) [11]. In real components' life, many events can damage the matrix, such as low velocity impacts [12,13] or machining [14] and the residual strength of these components strongly depends on the matrix properties. In order to compare efficiently a group of resins for CFRP a testing campaign that included only the most representative tests for the matrix behaviour was designed.

Moreover, to evaluate the exposure to harsh environmental conditions and high temperature exposure, several accelerated aging protocols were scheduled and mechanical properties were checked also after conditioning. Two sets of thermal oxidation conditioning were planned: a long steady exposure at elevated sub-Tg temperature and several short exposures at high temperature above Tg. Whereas the former is intended to stress the material to obtain the allowable loss factor over the whole lifetime of the wheel, the latter is intended for the durability and resistance against bursts of temperature due to hot spots that could appear on the wheel during critical sporadic events (e.g. during hard breaking). [15] For this campaign, out of plane shear tests and compression after impact loading were selected: resistance to compression was verified both in pristine condition following ASTM D3410 standard [16] and after impact by drop weight, according to ASTM Standard D7137 [17] (CAI test).

Impact tests were conducted according to ASTM D7136 [18] on an instrumented drop-weight machine [19] at different nominal energy levels (in the range 3–18 J).

Out of plane matrix shearing was tested in short beam geometry according to ASTM D2344 [20] (Inter Laminar Shear test, ILSS). in fact, the inter-laminar shear strength is a sensitive parameter for the evaluation of a class of composite materials, particularly to evaluate the modifications of the matrix after oxidative and degradation phenomena [21]. CAI and ILSS tests were performed on specimens in the post-cured condition and after accelerated aging protocols.

Table 2
Complete list of tests performed vs. aging conditioning.

Codename	Ageing Protocol		Resin system			Tests						
	Temperature [°C]	Time [h]	ER450	H2.2	H4	ILSS	Fatigue	Compressive	CAI	DMA	DSC	TGA
Ref	–	–	X	X	X	X	X	X	X	X	X	X
h360	180	360	X	X	X	X				X		
h720	180	720	X	X	X	X	X	X	X	X		
h1440	180	1440	X	X	X	X				X		
h2160	180	2160	X			X				X		
t200	200	72	X	X	X	X						
t210	210	72	X	X	X	X						
t220	220	72	X	X	X	X						
t230	230	72	X	X	X	X						
t240	240	72	X	X	X	X						
t250	250	72	X	X	X	X						

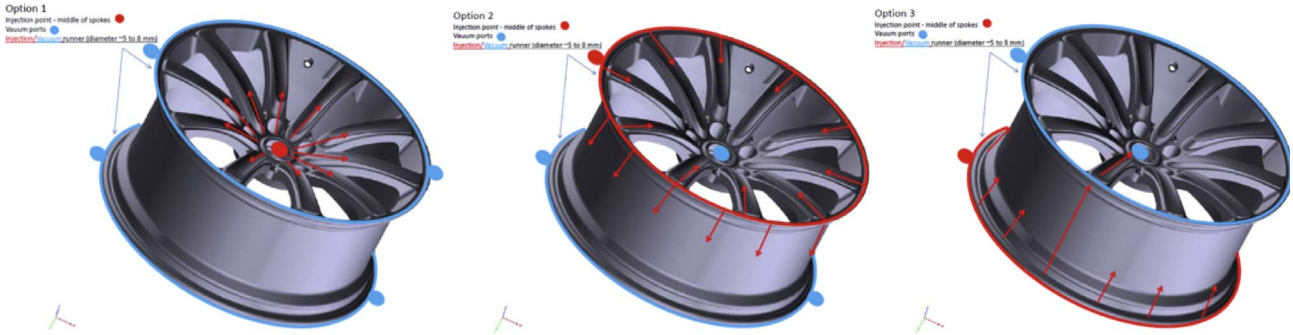

Fig. 3. Evaluation of different injection strategies through PAM-RTM FEM simulation.

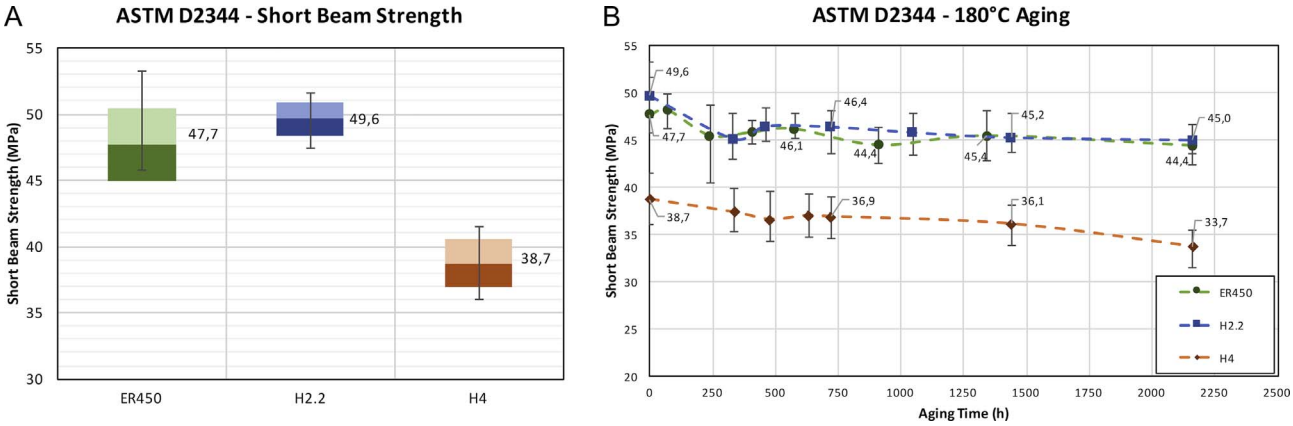

Fig. 4. a. ILSS tests result in the post cured condition. b. Evolution of ILSS with aging times at 180 °C continuously oxidative exposure.

A summary of the chemical and mechanical tested condition together with aging cycles are reported in Table 2.

2.3. FEM simulation of injection strategies

The costs for HP-RTM mould processing can be extremely high in particular if severe adjustment and re-working are required as a consequence of defects onset in the starting phase of production trials and process optimization. For this reason, a virtual simulation of the injection process was planned in order to identify, at the early stage of the mould design, all the possible critical issues. The ESI PAM-COMPOSITE suite was selected for the activity due to the presence of PAM-RTM module able to simulate the Resin Injection Technologies as already validated by the authors in previous works [7,10]. Starting point of the activity was the characterization of fibre permeability of the selected materials. Three different fibres were tested i.e. A: unidirectional fibre 12K T700 300 g/m^2, B: triaxial fibre (30/90/−30) 24K T700 300 g/m^2, C: Twill 2 × 2 fabric 12K T700 630 g/m^2. The permeability characterization was realized and analyzed as described by Weitzenbock in [22]. A sketch of the experimental equipment is reported in Fig. 3: the system has an internal cavity of 260 × 130 × 6.2 mm where plies of 220x130mm were placed with a stacking sequence able to produce a target fibre ratio of 55%. A pressure difference between injection and vent of 0.4 bar was applied. Plies were put in 0°, 45° and 90° direction in order to retrieve the Principal Permeability values (K1 and K2) from the local permeability (K0, K45, K90) data [23–24]. The test was repeated 3 times for each fibre thus bringing to 9 the number of the tests to be performed for the characterization of each material.

The values obtained from permeability characterization were used for the simulation of the injection strategies [25]. Values of resin Newtonian viscosity were provided by technical datasheets of the supplier. Fig. 3 reports the sketch of 3 different evaluated injection strategies: strategy a) realizes the injection in the central hub with vacuum applied around the top and bottom runner, strategy b) realizes the injection in the top runner with vacuum applied in the hub and in the bottom runner, while strategy c) realizes the injection in the bottom runner with vacuum applied in the top runner and in the hub. Results were investigated under constant resin flow rate in term of filling time, filling factor (for possible dry spots localization), maximum injection pressure and local pressure in several critical locations by changing fibre types and resin.

3. Results and discussion

3.1. Mechanical and durability testing

Mechanical tests and environmental aging protocols were first realized. Out of plane matrix shearing static tests (Inter Laminar Shear test, ILSS ASTM D2344) were realized on the full experimental plan while ILSS fatigue, compressive (ASTM D3410) and Compression After Impact (CAI, ASTM D7136-D7137) tests were realized on selected conditions as reported in Table 2.

3.1.1. Inter laminar shear strength

Fig. 4a reports the results of out of plane matrix shearing static tests (Static ILSS) for the three analyzed resin systems in the post-cured condition. The error bar indicates the scatter over the 7 repetitions while the color bar reports the standard deviation. System H2.2 anhydride behaved comparably or slightly better respect to ER450 reference system while system H4 amine exhibited reduced mechanical proprieties of around 20%. Fig. 4b shows the trend of the ILSS average strengths after aging at 180 °C for different exposure times. The H2.2 and ER450 systems had a completely overlapping behavior (taking into consideration the data scattering), with a limited initial decreasing of 5 MPa in the first 250 h aging then stabilizing at a 45 MPa strength level within 2160 h (3 months) of continuous exposure to the aging

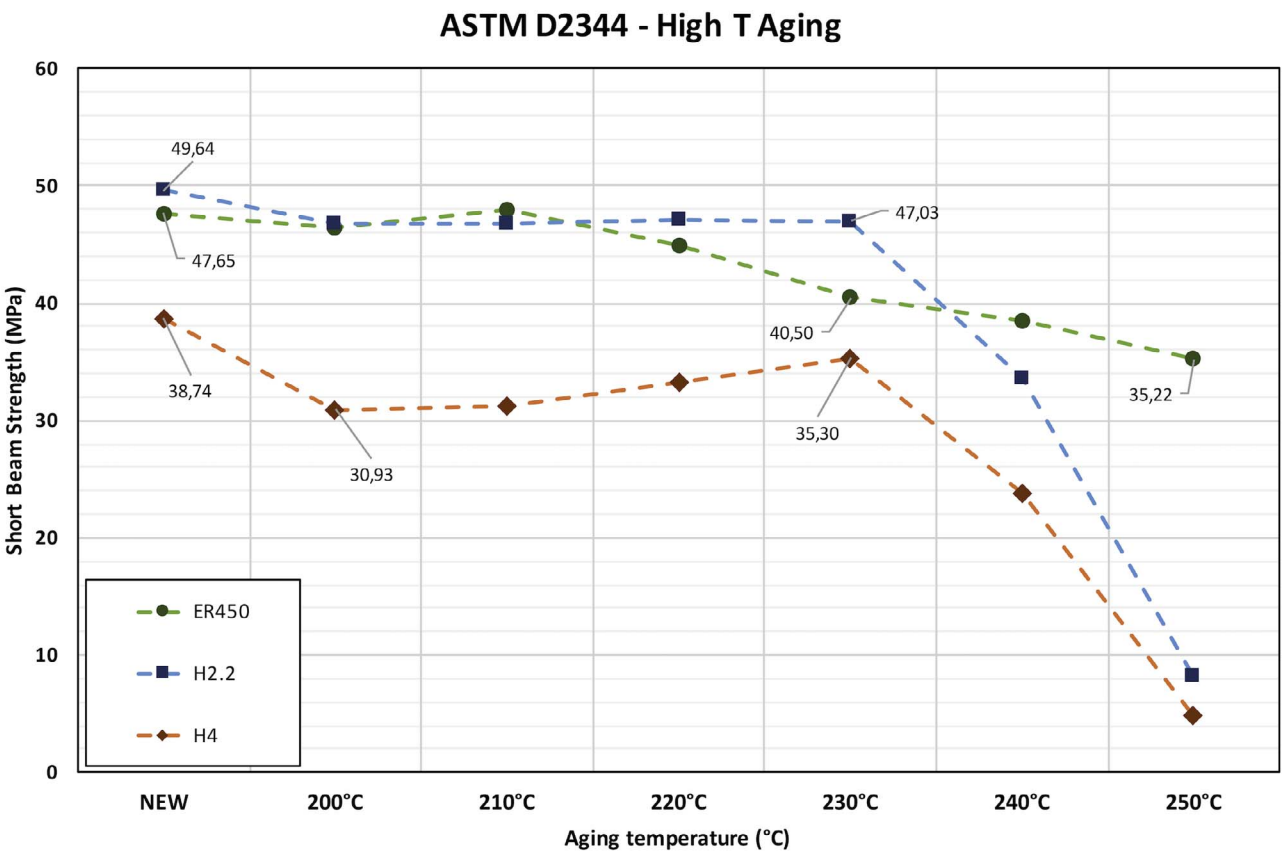

Fig. 5. ILSS tests result over aging temperature at constant exposure time (72 h).

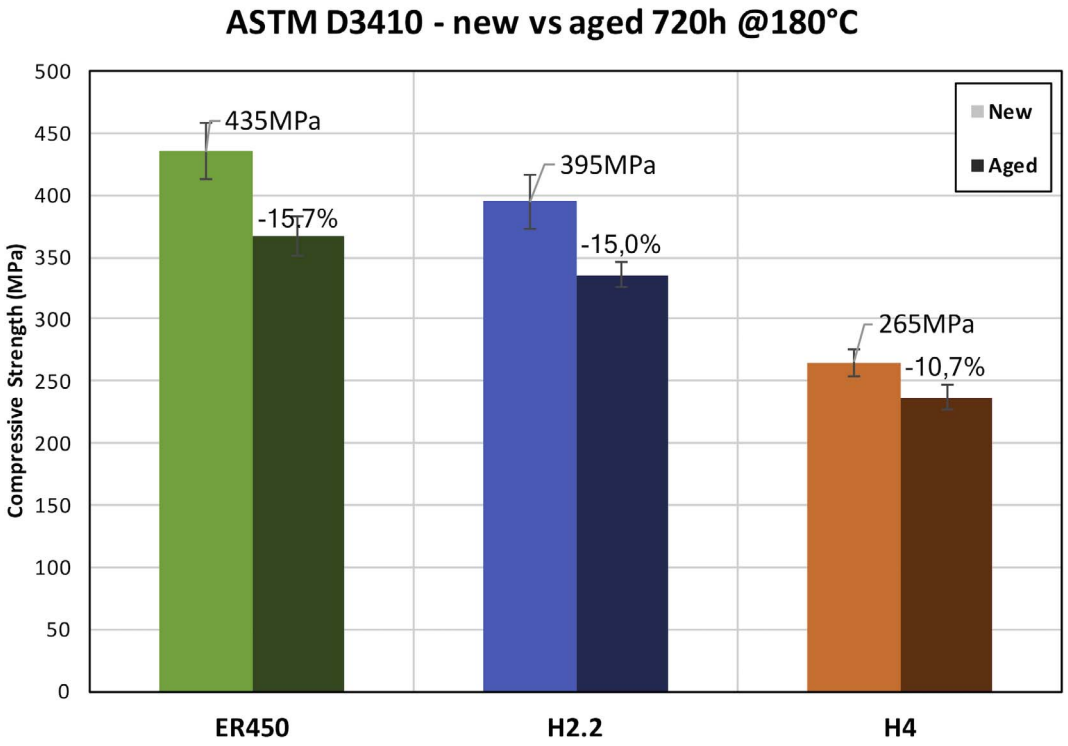

Fig. 6. Compressive strength of post-cured samples compared with aged condition at 180 °C for 720 h.

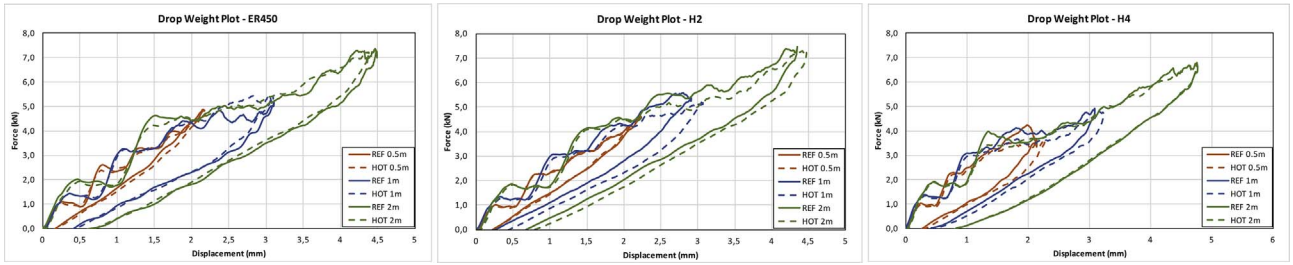

Fig. 7. Impact Load-Displacement curves: comparison between reference and hot aged conditions for the different resin systems.

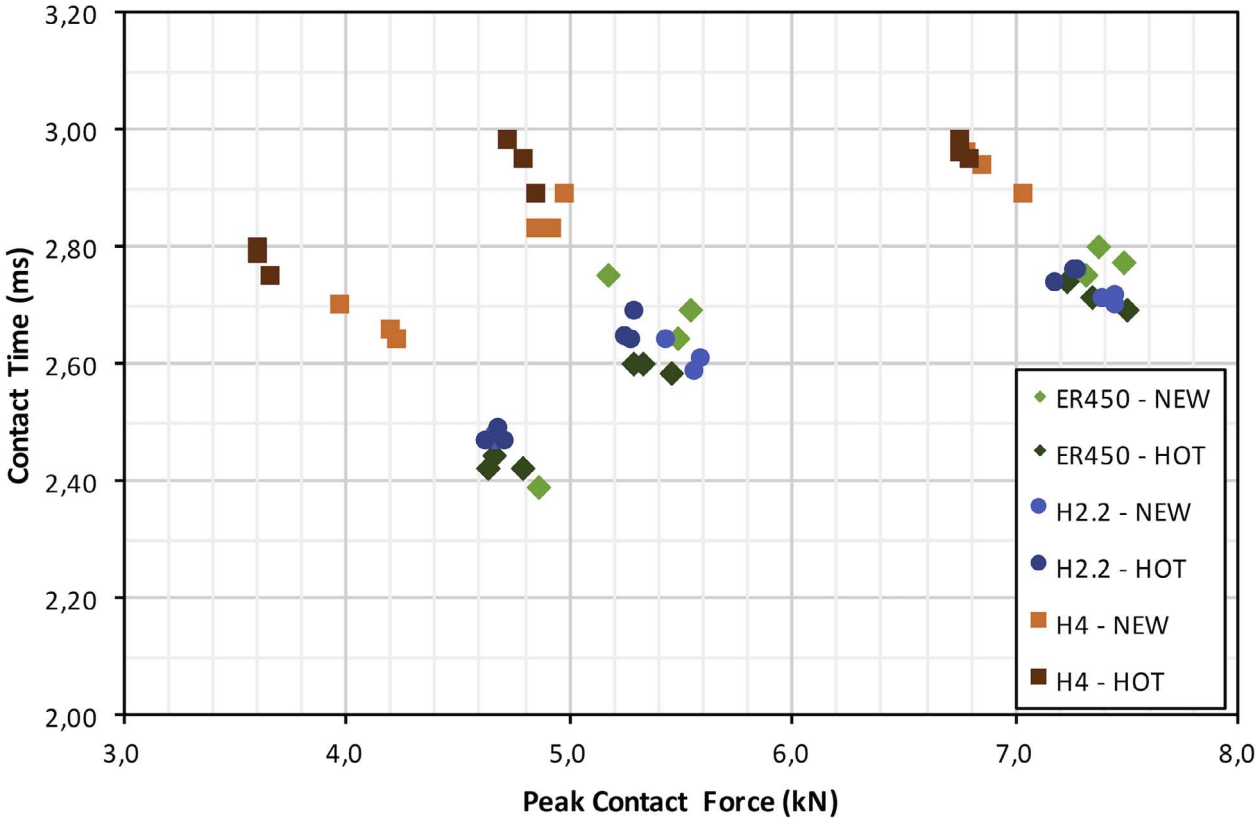

Fig. 8. Detail of impact events, 0.5 m (left), 1 m (centre) and 2 m (right) impact heights.

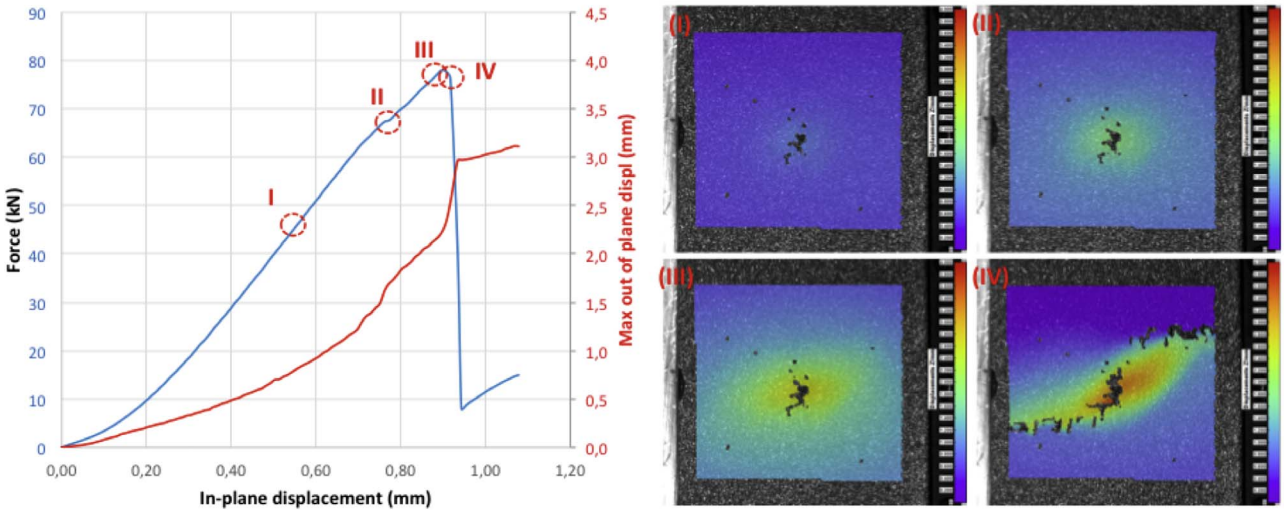

Fig. 9. a) Compressive force and bending displacement as a function of the in-plane displacement, b) DIC images corresponding to the indicated point on the graph a).

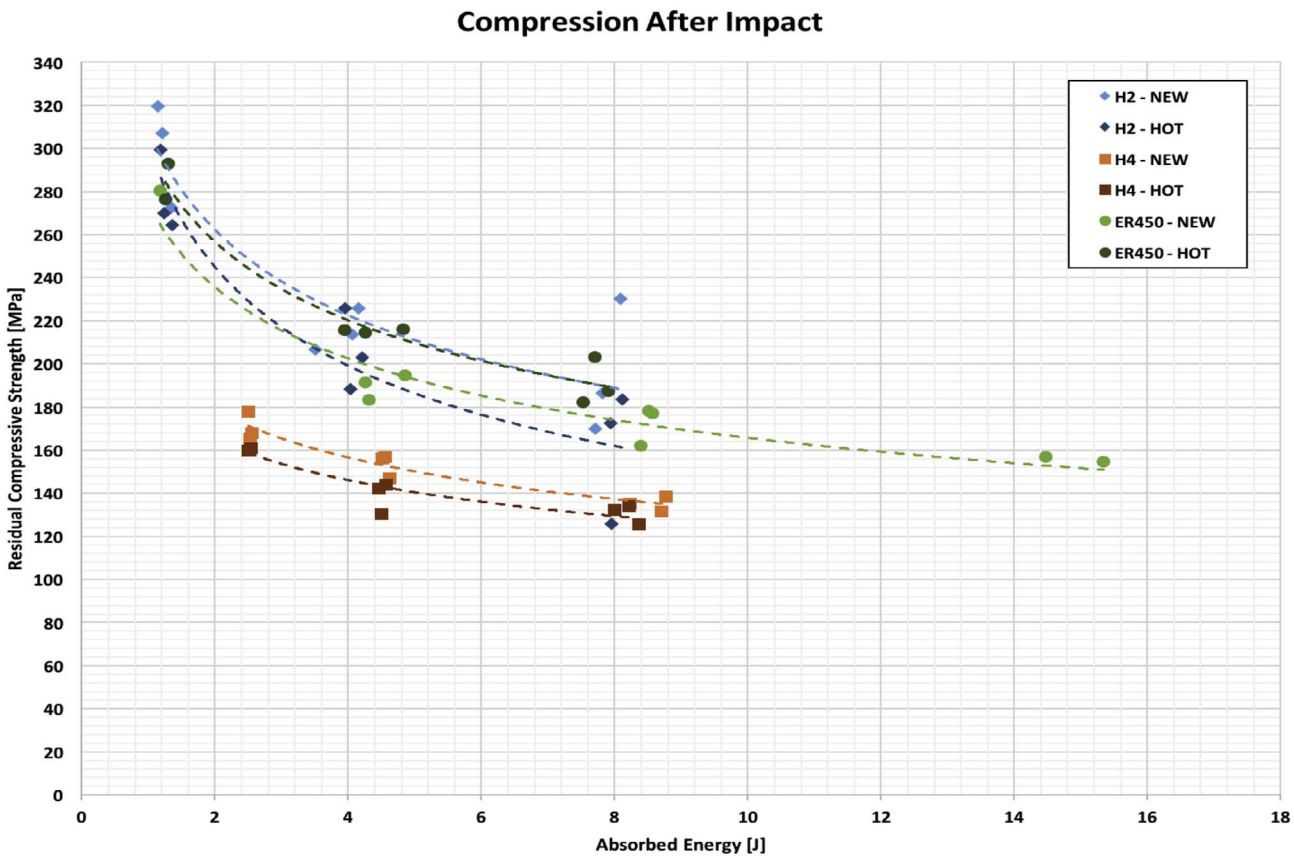

Fig. 10. Compression after impact strengths on post-cured and thermal aged specimens.

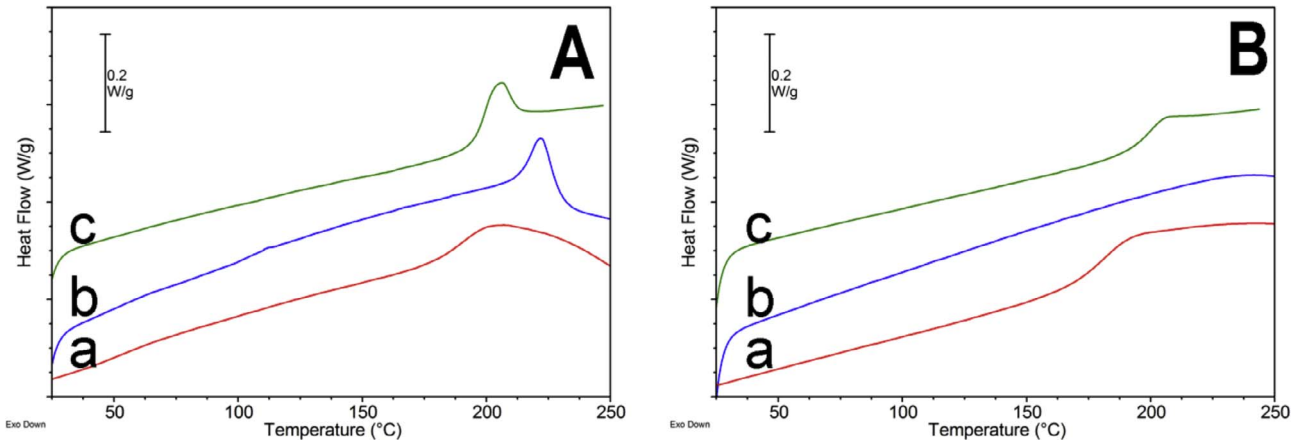

Fig. 11. DSC thermograms of the first (A) and second (B) heating scans of: a) ER450 (red), b) H4 (blue) and c) H2.2 (green).

temperature. The H4 system confirmed the lower values of strength obtained at the post-cured condition also during thermal aging. It showed a lower decrement in the first week of aging respect to the other systems, but the onset of a further decrement was visible after 1500 h of aging.

Completely different results were obtained when the materials were aged at higher temperature, above T_g, even for a shorter exposure time (72 h) as reported in Fig. 5. Here the effects are severe, as several phenomena occurred when the material was exposed at these temperatures: the permeability to oxygen was higher, thus oxidative effects were deeply accelerated, the internal stresses were recovered at high temperature, then to be reintroduced in the form of thermal shrinkage during cooling down. For system H2.2 there was almost no change after 72 h exposure up to 230 °C, but when this temperature was overcome static strength abruptly decreased to an almost zero value at 250 °C exposure. Reference system ER450 behaved comparably respect to H2.2 up to 220° exposure temperature, then it started decreasing its strength but with a less critical decrement thus keeping at 250°c exposure a residual strength of 35 MPa (it kept a 75% of the initial strength). System H4 started immediately its decrease: at 200 °C oxidation temperature specimen strength was as low as it was at 1500 h exposure at 180 °C. A slight recovery is then visible in the range 210–230°, possibly due to some post-curing phenomena occurring above T_g which helps raising the glass transition of the system during the thermal treatment, followed by an abrupt decrement as was present for H2.2 system.

3.1.2. Compression tests

Compressive tests were performed following ASTM D3410 standard,

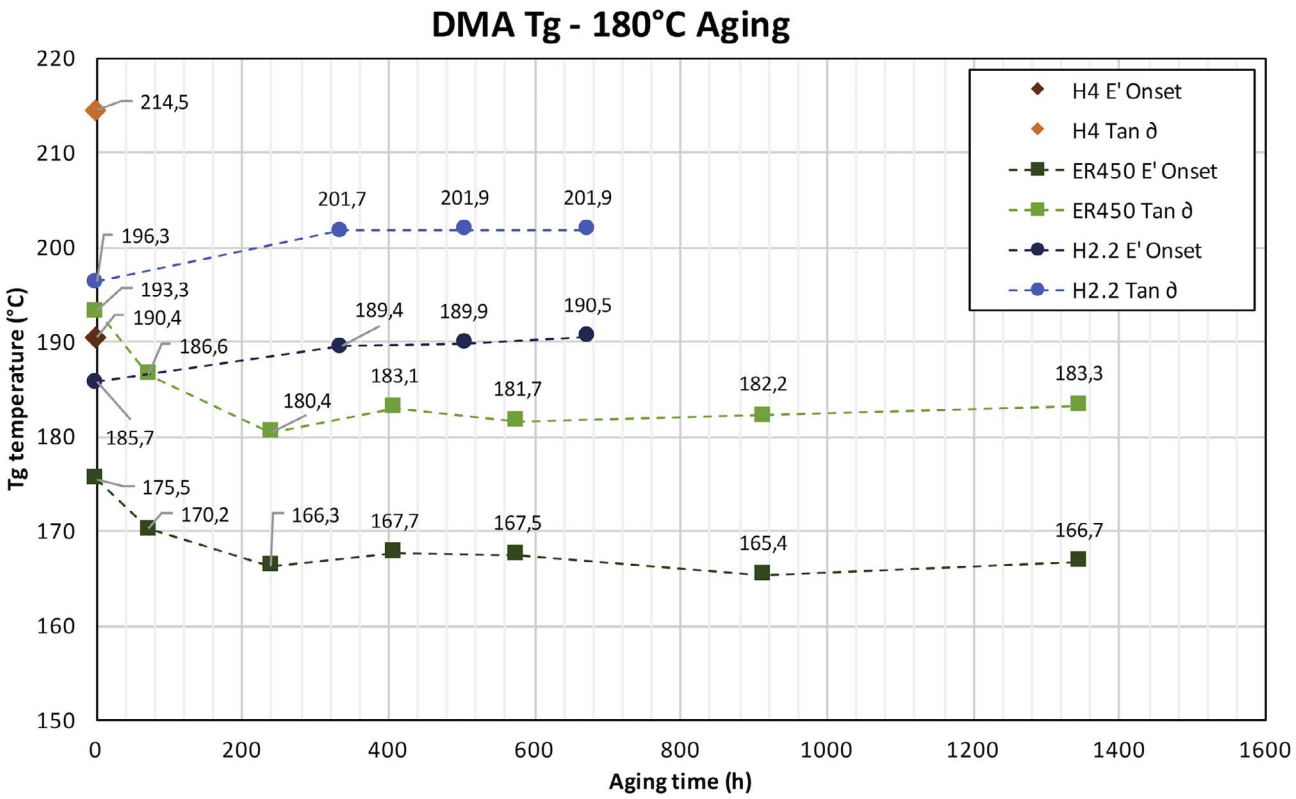

Fig. 12. Glass transition, evaluated both E′ onset ($T\alpha_{E'}$, extrapolation of the first storage modulus E′ loss) and tan δ (taken as the peak of the damping factor), displayed as a function of aging time at 180 °C.

Table 3
Thermal properties of the investigated resin systems.

	DSC		TGA	DMA	
	$T_{g\ I\ scan}$ (°C)	$T_{g\ II\ scan}$ (°C)	T_d (°C)	$T\alpha_{E'}$ (°C)	$T\alpha_{tan\delta}$ (°C)
ER450	n.a.	178	294	175	193
H2.2	196	197	282	186	196
H4	n.a.	n.a.	272	190	214

with 25 mm gage length and 15 mm specimen width. Only the tests that resulted in acceptable failure mechanism were considered in the calculation of average strength (Fig. 6). Data indicated that the pre-preg system can sustain the highest load before collapsing, with the H2.2 system not far below. The third system analyzed, in analogy with the results from ILSS tests, was 30% less resistant. The effect of thermal oxidation has a similar impact on the two best performing systems (ER450 and H2.2), while the third shows a less prominent effect.

3.1.3. Impact loading

In the instrumented drop weight test a 1.3 kg mass impactor was used. Different nominal energy levels were obtained by impact heights: 0.5, 1 and 2 m (3m only for ER450). The actual kinetic energy was measured by means of a laser device before impact and after rebound.

Examples of the Load-displacement curves obtained are shown in Fig. 7, being the area inside the curve equal to the energy absorbed by the specimen during the impact event.

In Fig. 8 a summary of the main features of the impact tests, i.e. peak force and time duration of the contact, are shown. It is quite evident that system H4 behaved differently from the other two, having both lower peak forces and higher contact times for all the nominal energy levels considered. This is an indication of higher damage level, respect to the other two systems.

3.1.4. Compression after impact

The CAI strength was measured on ASTM standard 100 × 150 mm specimen. The possible global plate buckling, that would invalidate the test, was monitored during the CAI test by means of a Digital Image Correlation device, as shown as an example in Fig. 9.

A further evidence of a higher damage level of system H4 can be found also in the graph of Fig. 10, in which the residual compressive strength (MPa) after impact is plotted versus the energy absorbed by the specimen during the impact. The absorbed energy was calculated from the difference between the final kinetic energy immediately before contact and the re-bounce energy just after impact.

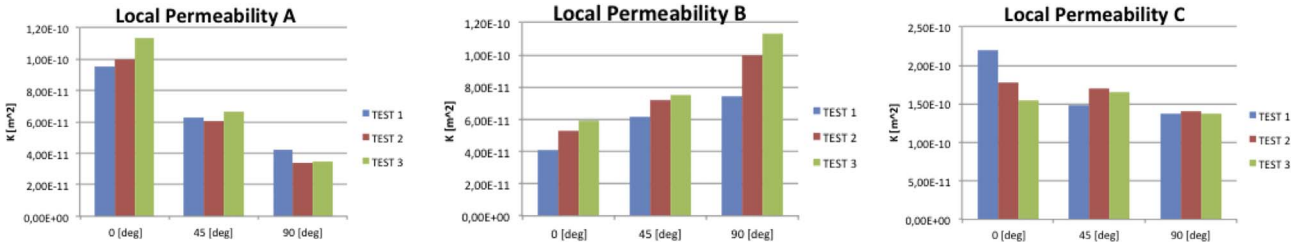

Fig. 13. Local permeability for materials A-unidirectional fibre 12 K T700 300 g/m^2, triaxial fibre (30/90/-30) 24 K T700 300 g/m^2, C-Twill 2x2 fabric 12 K T700 630 g/m^2.

Table 4
Experimentally determined local and principal permeability values.

	Local permeability [m^2]			Principal permeability [m^2]			Angle [rad]	Density [kg/m^3]
	K0	K45	K90	K1	K2	K3	Phi	Rho
Plies A	1.03E−10	6.33E−11	3.70E−11	1.03E−10	3.63E−11	1.00E−09	0.0985	1800
Plies B	5.09E−11	6.95E−11	9.59E−11	9.62E−11	5.06E−11	1.00E−10	1.484	1800
Plies C	1.84E−10	1.61E−10	1.38E−10	1.84E−10	1.38E−10	1.00E−09	0.0118	1800

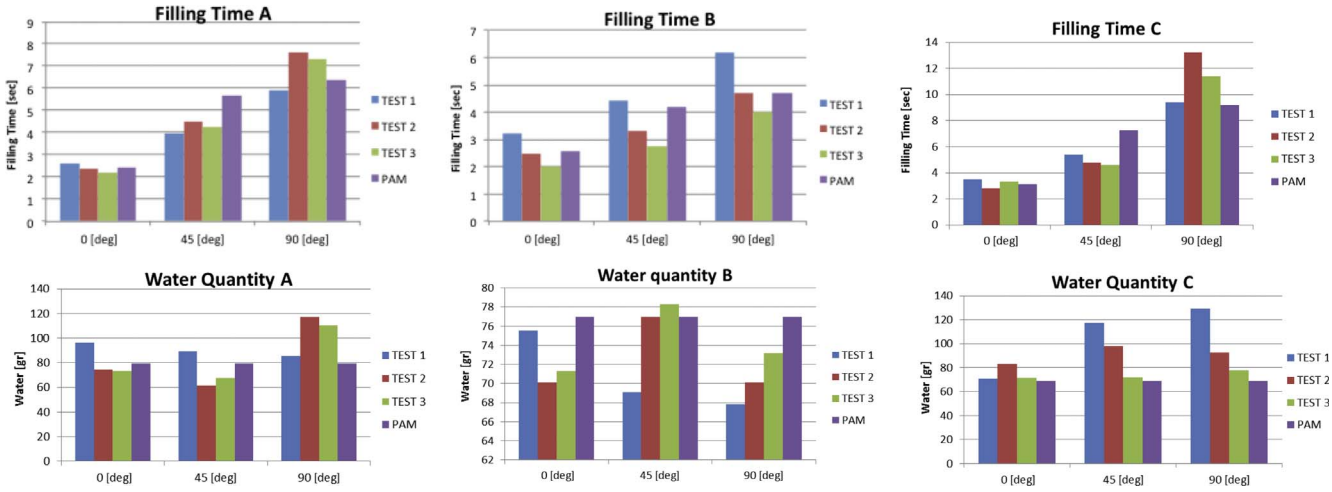

Fig. 14. Comparison of experimental and simulated filling time and injected resin quantity.

Table 5
Summary of FEM injection strategies evaluation.

Strategy	Flow Rate [m^3/s]	Filling Time [s]	Max. Pressure [bar]	Dry Spots
a)	3.33e−5	52	21	–
a)	4.45e−5	39	28	–
b)	3.33e−5	51	7.6	Intersecting flows at spokes
b)	4.45e−5	39	10	Intersecting flows at spokes
c)	3.33e−5	50	17	At hub behind the holes
c)	4.45e−5	38	22	At hub behind the holes

In the post-cured conditions, in contradiction with the compressive tests made following D3410 standard, H2.2 had the highest resistance after all impacts, followed by ER450 and by H4. After 1 month aging @ 180 °C the behaviour of the three systems was quite different: the two RTM systems reduced their respective residual strength, in particular H4 lost about 10 MPa independently from the Impact Energy, while H2.2 showed negligible effects of aging when impacted at lower energy, while lost up to 30 MPa at higher impacts energies. Surprisingly ER450 system increased its residual strength of an average value of 10 MPa at all impact energies.

It is interesting to notice how the system H4 consistently showed higher absorbed energies at every impact height. This is particularly evident at the lowest impact level (0.5 m), for which the energy absorbed during impact was more than double, compared with both ER450 and H2.2 systems.

3.1.5. *Differential scanning calorimetry and dynamical mechanical analysis*

Before any additional temperature aging treatment, all the specimens were analyzed by DSC in order to assess the presence of residual exothermic phenomena when brought at high temperature, symptom of uncomplete cure and, when detectable, the stability of the T_g after a second heating scan. This assessment was carried out with the aim of evaluating the thermal behavior in highly demanding thermal conditions, where the material should guarantee a good performance, even if just for a limited time span. As can be seen in Fig. 11, all the investigated sample did not show any exotherm below 200 °C, accounting for a fairly high thermal stability, while only H2.2 appeared to be fully cured (Fig 12).

Both ER450 and H4 displays in the first scan some hint of exothermic events, processes typical of crosslinking, above 200 °C, namely just above the glass transition, i.e. when the system regains mobility and the ability to start reacting again, thus accounting for both being vitrified systems. Since TGA analysis shows degradation temperature (T_d), determined as the temperature at which a 1% weight loss occurs, well above 270 °C, it can be safely ruled out that such exotherms are due to degradation processes. Hence some additional reactions might occur during the first heating in the DSC. Moreover, due to some enthalpic relaxation, it is not possible to safely evaluate the glass transition temperature for the investigated resins during the first scan, i.e. representing the situation as is. It is however possible to observe that ER450 Tg is just slightly affected by the first heating run, while H4 system shows first a physical aging located around 220 °C and almost no transition within 250 °C in the second scan. This difference well supports the previous ILSS results, where H4 displays some increase in propertied during thermal treatments around 210–230 °C, where the curing is significantly pushed. Owing to the inability of DSC thermograms to provide reliable T_g, the glass transition has thus been determined via DMA as reported in Table 3, assessing both E′ onset ($T\alpha_{E'}$, extrapolation of the first storage modulus E′ loss) and tan δ ($T\alpha_{tan\delta}$, taken as the peak of the damping factor). The span between the two values is an indication of the width of the relaxation phenomenon. While the H4 resin system appear to be the one with the highest performances as regarding the glass transition, the gap between $T\alpha_{E'}$ onset and $T\alpha_{tan\delta}$ is quite relevant, accounting for an unstable behavior possibly due to the uncomplete curing of the system. The H2.2 resin, instead, though showing a glass transition phenomenon generally located at lower temperatures, display values closer on to the other, accounting

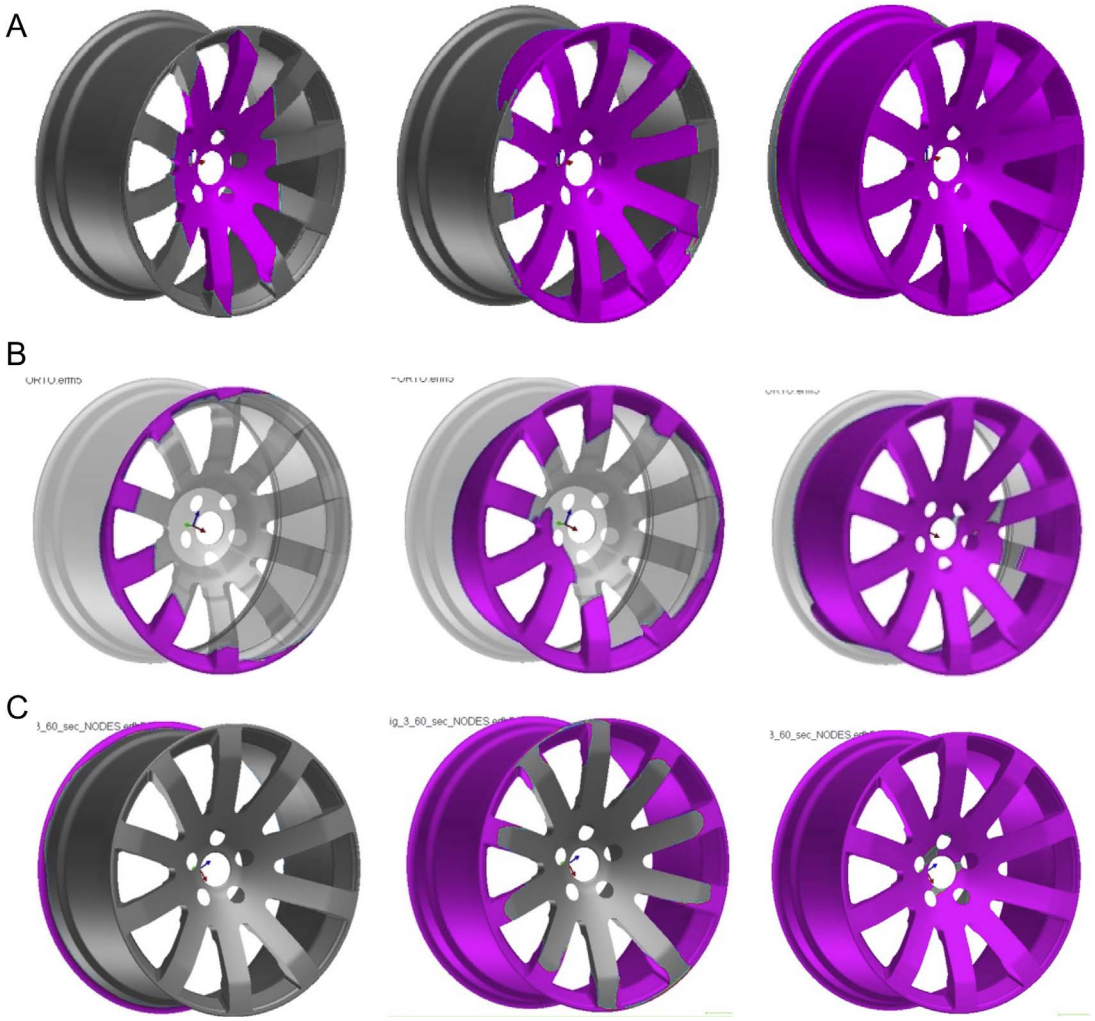

Fig. 15. Evolution of filling factor with the Strategy a). Evolution of filling factor with the three Strategy b). Evolution of filling factor with the Strategy c).

for a system which is more stable. In order to assess the stability of these systems in terms of time and temperature, DMA measurements were also carried out after aging at high temperature (Fig. 13). In these aged conditions, ER450 shows an initial decrease in the position of the main dissipation phenomenon, then reaching stability with aging times over 200hrs, while system H2.2 shows a slight initial increase in T_g followed by a stabilization after more than 300hrs aging. Owing to the indication of incomplete reaction and the poor mechanical proprieties displayed by H4 system, no further thermal treatment was applied to this resin. In Table 3 the details of the thermal properties are reported.

3.2. FEM simulation of injection strategies

Local permeability results for the three selected fibre types are reported in Fig. 13 including the scattering over three repetitions. Table 4 reports the values of local and principal permeability to be inserted in the FEM code.

FEM simulation of the permeability determination test showed a good agreement with experimental values providing an average error in filling time and injected resin quantity below 5% (Fig. 14).

Next step of the simulation activity was the evaluation of different injection strategies as already detailed in the previous paragraphs: strategy a) realizes the injection in the central hub with vacuum applied around the top and bottom runner, strategy b) realizes the injection in the top runner with vacuum applied in the hub and in the bottom runner, while strategy c) realizes the injection in the bottom runner with vacuum applied in the top runner and in the hub (Fig. 14a–c). Two resin flow rates were considered $3.3e-5\,m^3/s$ and $4.45\,m^3/s$ in the prediction of filling time and maximum pressure; the computed values are reported in Table 5. The simulations allowed to evidence and compare the evolution of mould filling (Fig. 15a–c), the required injection times and the localization of possible dry spots or intersecting flows. Moreover, the simulation results numerically predicted the evolution of the pressure in the mould at different stages of the injection together with the estimation of maximum pressure required to the injection system in order to complete the filling (max. pressure reported in Table 5).

Although the resin flow path is quite different in the three strategies (longer in strategy a) and c), shorter in strategy b)) the computed filling time is only flow rate dependent (around 51 s for lower flow rate, around 39 s for higher flow rate). Indeed by selecting an injection method with a constant flow rate (instead of at constant pressure for example), volume of material to be filled is equal in the three strategies and consequently also injection times are almost identical. Using a constant resin injection flow rate, maximum pressures with the 3 strategies become quite different: higher flow rates require higher pressures and each injection strategy requires a different amount of maximum pressure. Strategy b) is the one requiring lower pressure since the path to be covered by the resin is shorter, while strategy a) and c) led to different pressures although the path is identical in the two solutions (just reversed).

Finally, FEM simulation was able to foresee onset of possible dry

spots (like in strategies c) or the intersection of different flow fronts within the component (like in strategy b)) thus leading to possible porosity or air/gas entrapment thus allowing the identification of tailored solutions in order to overcome them.

4. Conclusions

The preliminary results showed that the production a full carbon wheel through an automated preforming and HP-RTM process, that is the aim of the CARIM project, was feasible and leaded to a sharp reduction of manufacturing times. Moreover, the resin infusion system H2.2 (anhydride) could be a valid substitute of the ER450 (pre-preg) for the production of a full carbon wheel through HP-RTM processing with no decrement of material mechanical performances.

System H2.2 had, respect to ER450:

- an inter-laminar shear static strength comparable or even slightly superior;
- a limited decrease of ILSS over high temperature exposure below Tg but also a safe behaviour when higher hot burst may occur;
- It maintained a good failure strength also under compressive loads and the decrease related to damaging impacts was comparable respect to ER450 at both post-cured and thermal aging conditions;
- It exhibited a higher glass transition temperature onset ($T\alpha_{E'}$) that initially increased during thermal aging remaining then stable at 190 °C;

System H4 showed a reduced mechanical performance respect to H2.2 and ER450 although a greater thermal stability was found.

Finally, FEM simulations allowed to properly predict injection phase with particular reference to mould and process design thus evidencing strength and weakness points and allowing the solution of critical aspects at an early design stage.

Further results and the actual manufacturing process, including the fibre preform lay-out and the rims qualification mechanical test, will be published after the end of the project.

Acknowledgments

The research was funded by European Commission in the Horizon 2020 research and innovation programme, under H2020-FTIPilot-2015-1 (Grant Agreement no. 690915). The authors thank DR. Tommaso Brugo for the assistance in the Impact and CAI test.

References

[1] Mock P. EU CO2 standards for passenger cars and light-commercial vehicles. International Council on Clean Transportation (ICCT). Available on line from theicct.org; 2014.
[2] Badeghar T. Lightening up with carbon fiber-reinforced plastics, markets and markets; January 2016.
[3] Chung DDL. Processing-structure-property relationships of continuous carbon fiber polymer-matrix composites. Mater Sci Eng R Rep 2017;113:1–29.
[4] Rosenberg P, Chaudhari R, Albrecht P, Karcher M, Henning F. Effects of Process parameters on cavity pressure and components performance in high-pressure RTM process variants. In: 14th-annual SPE Automotive Composites Conference & Exhibition, 2014; Novi (MI), USA.
[5] Rosenberg P, Thoma B. Henning F. Characterization of epoxy and polyurethane resin systems for manufacturing of high-performance composites in high-pressure RTM process. In: 15th-annual SPE Automotive Composites Conference & Exhibition; 2015: Novi (MI), USA.
[6] Laurenzi S, Marchetti M. Advanced Composite Materials by Resin Transfer Molding for Aerospace Applications, Composites and Their Properties. Prof. Ning Hu (Ed.), InTech; 2012. DOI: 10.5772/48172.
[7] Poodts E, Minak G, Mazzocchetti L, Giorgini L. Fabrication, process simulation and testing of a thick CFRP component using the RTM process. Compos B Eng 2014;56:673–80.
[8] Rosenberg P, Chaudhari R, Karcher M, Henning F, Elsner P. Investigating cavity pressure behavior in high-pressure RTM process variants. AIP Conf Proc 2014;1593:463–6.
[9] http://www.carimproject.eu.
[10] Poodts E, Minak G, Dolcini E, Donati L. FE analysis and production experience of a sandwich structure component manufactured by means of vacuum assisted resin infusion process. Compos B Eng 2013;53:179–86.
[11] Talreja R. Damage and fatigue in composites – a personal account. Compos Sci Technol 2008;68(13):2585–91.
[12] Minak G, Abrate S, Ghelli D, Panciroli R, Zucchelli A. Low-velocity impact on carbon/epoxy tubes subjected to torque – experimental results, analytical models and FEM analysis. Compos Struct 2010;92(3):623–32.
[13] Minak G, Abrate S, Ghelli D, Panciroli R, Zucchelli A. Residual torsional strength after impact of CFRP tubes. Compos B Eng 2010;41(8):637–45.
[14] Zarif Karimi N, Heidary H, Minak G, Ahmadi M. Effect of the drilling process on the compression behavior of glass/epoxy laminates. Compos Struct 2013;98:59–68.
[15] Chandra Ray B, Rathore D. Durability and integrity studies of environmentally conditioned interfaces in fibrous polymeric composites: critical concepts and comments. Adv Colloid Interface Sci 2014;209:68–83.
[16] ASTM D3410/D3410M-16. Standard test method for compressive properties of polymer matrix composite materials with unsupported gage section by shear loading. ASTM International: West Conshohocken, PA; 2016, www.astm.org.
[17] ASTM D7137/D7137M-17. Standard test method for compressive residual strength properties of damaged polymer matrix composite plates. ASTM International: West Conshohocken, PA; 2017. www.astm.org.
[18] ASTM D7136/D7136M-2015. Standard test method for measuring the damage resistance of a fiber-reinforced polymer matrix composite to a drop-weight impact event. ASTM International: West Conshohocken, PA; 2015. www.astm.org.
[19] Ghelli D, Minak G. Low velocity impact and compression after impact tests on thin carbon/epoxy laminates. Compos B Eng 2011;42(7):2067–79.
[20] ASTM D2344/D2344M-16. Standard test method for short-beam strength of polymer matrix composite materials and their laminates. ASTM International: West Conshohocken, PA; 2016. www.astm.org.
[21] Wolfrum J, Eibl S, Lietch L. Rapid evaluation of long-term thermal degradation of carbon fibre epoxy composites. Compos Sci Technol 2009;69(3–4):523–30.
[22] Weitzenbock JR, Shenoi RA, Wilson PA. A unified approach to determine principal permeability of fibrous porous media. Polym Compos 2002;23(6):1132–50.
[23] Arbter R, Beraud JM, Binetruy C, Bizet L, Bréard J, Comas-Cardona S, Demaria C, Endruweit A, Ermanni P, Gommer F, Hasanovic S, Henrat P, Klunker F, Laine B, Lavanchy S, Lomov SV, Long A, Michaud V, Morren G, Ruiz E, Sol H, Trochu F, Verleye B, Wietgrefe M, Wu W, Ziegmann G. Experimental determination of the permeability of textiles: a benchmark exercise. Compos A Appl Sci Manuf 2011;42(9):1157–68.
[24] Vernet N, Ruiz E, Advani S, Alms JB, Aubert M, Barburski M, Barari B, Beraud JM, Berg DC, Correia N, Danzi M, Delavière T, Dickert M, Di Fratta C, Endruweit A, Ermanni P, Francucci G, Garcia JA, George A, Hahn C, Klunker F, Lomov SV, Long A, Louis B, Maldonado J, Meier R, Michaud V, Perrin H, Pillai K, Rodriguez E, Trochu F, Verheyden S, Wietgrefe M, Xiong W, Zaremba S, Ziegmann G. Experimental determination of the permeability of engineering textiles: benchmark II. Compos A Appl Sci Manuf 2014;61:172–84.
[25] Demaría C, Ruiz E, Trochu F. In-plane anisotropic permeability characterization of deformed woven fabrics by unidirectional injection. Part II: prediction model and numerical simulations. Polym Compos 2007;28:812–27.